MEG Source Imaging Using Multipolar Expansions

John C. Mosher[1], Richard M. Leahy[2], David W. Shattuck[2], and Sylvain Baillet[2]

[1] Los Alamos National Laboratory, MS D454
Los Alamos, New Mexico USA 87545
mosher@LANL.Gov
[2] Signal and Image Processing Institute
University of Southern California
Los Angeles, California USA 90089-2564
{leahy, shattuck, silvin}@sipi.usc.edu

Abstract. We describe the use of truncated multipolar expansions for producing dynamic images of cortical neural activation from measurements of the magnetoencephalogram. We use a signal-subspace method to find the locations of a set of multipolar sources, each of which represents a region of activity in the cerebral cortex. Our method builds up an estimate of the sources in a recursive manner, i.e. we first search for point current dipoles, then magnetic dipoles, and finally first order multipoles. The dynamic behavior of these sources is then computed using a linear fit to the spatiotemporal data. The final step in the procedure is to map each of the multipolar sources into an equivalent distributed source on the cortical surface. The method is demonstrated through a Monte Carlo simulation.

1 Introduction

Magnetoencephalography (MEG) data are measurements of the magnetic fields produced by neural current sources within the brain. The problem of estimating these sources is highly ill-posed due to the inherent ambiguities in the associated quasistatic electromagnetic inverse problem, the limited number of spatial measurements and significant noise levels. To overcome these problems, constraints can be placed on the location and form of the current sources. Mapping studies using direct electrical measurements, fMRI and PET reveal discrete focal areas of strong activation within the cortex that are associated with specific cognitive, sensory and motor activities. Consequently, a plausible model for the current generators in an event related study consists of a number of focal cortical regions each of which has an associated time course [12]. The MEG inverse problem requires estimation of the spatial and temporal characteristics of these sources.

There are two major classes of methods for solving the MEG inverse problem which we will refer to as "imaging" and "model based." The imaging methods typically constrain sources to a tessellated representation of the cortex, assume

A. Kuba et al. (Eds.): IPMI'99, LNCS 1613, pp. 15–28, 1999.

an elemental current source in each area element, and solve the linear inverse problem that relates these current sources to the measured magnetic field. Accurate tessellations of the cortex require on the order of 10^5 elements. Since the maximum number of MEG sensors in the current generation of whole head MEG system is approximately 300, the problem is highly underdetermined. By using regularized linear methods based on minimizing a weighted L_2-norm on the image, we can produce unique stable solutions [11,14]. Unfortunately, these methods tend to produce very smooth solutions that are inconsistent with the focal model described above. Many nonlinear algorithms have been proposed that attempt to avoid this oversmoothing problem. While they have met with some success, the cost functions required to achieve more focal solutions are usually highly nonconvex and computation times can be very high, e.g. [1,11].

The model-based methods assume a specific parametric form for the sources. By far the most widely used models in MEG are multiple current dipoles [4,9,12]. These assume that the neural sources are relatively small in number and each sufficiently focal that they can be represented by a few equivalent current dipoles with unknown locations and orientations. Parametric methods can be extended to model the temporal correlation expected in the solutions through fitting the multiple dipole model to the entire data set and estimating the time course for each estimated dipole location. As with the nonlinear imaging methods, the cost functions are nonconvex. Signal subspace based methods such as MUSIC or RAP-MUSIC [7,8,9] can be used to rapidly locate the sources in a sequential fashion and avoid the problem of trapping in local minima.

The equivalent current dipole model is directly interpretable as a current element restricted to the cortical surface. As discussed in [10], the dipole may also represent locally distributed sources that are not necessarily restricted to a single point. However, one of the perceived key limitations is that these distributed sources may not be adequately represented by the dipole model. This problem was one of the prime motivations for the development of the imaging approaches. An alternative solution is to remain within the model-based framework but to broaden the model to allow parametric representations of distributed sources. The multipolar expansion provides a natural framework for generating these models. The multipolar expansions are formed using a Taylor series representation of the magnetic field equations. If the expansion point is chosen near the center of a distributed source, then the contribution of higher order terms will drop off rapidly as the distance from the source to the sensor increases. Using this framework we expand the set of sources to include magnetic dipoles and first order multipoles. These sources are able to represent the field from a distributed source more accurately than is the current dipole. While the idea of using multipolar expansions in MEG source modeling is not new, the approach has generally seen only limited used in magnetocardiography, e.g. [6,15].

The parameters of the estimated higher-order multipolar terms are not easily related to the actual physiological processes that produce the MEG signals. We describe here a two-stage procedure in which we first estimate the locations and parameters of the multiple multipoles, then relate each of the multipoles to

equivalent cortical sources. The method described here for estimating the location and moment parameters of these multipolar representations is an extension of the RAP-MUSIC method developed in [8] for localizing current dipoles. The algorithm recursively builds a model for the current source configuration by first testing for the presence of point current dipoles, then magnetic dipoles, and finally first order multipoles. In this way the model order and complexity is gradually increased until the combined estimated sources adequately explain the data.

In the cortical re-mapping stage, we find regions of cortex in the vicinity of the parametric source on which we fit current distributions consistent with the fields associated with each estimated multipole. The final result is then a dynamic image of current activity mapped onto a tessellated representation of the cortex which reveals the time varying behavior at the various locations on the cerebral cortex activated during a particular experiment.

2 Multipolar Source Modeling

2.1 Multipolar Expansions

The relationship between the measured magnetic field and the current sources is determined by the quasistatic form of Maxwell's equations. In the special case in which the head is modeled as a set of concentric nested spheres, each with uniform and isotropic conductivity, there is a simple integral equation that relates the external magnetic field to the current sources. We use this result to derive the multipolar expansion. We include details only for the case where measurements are made of the radial component of the magnetic field. They extend directly both to the case of non-radial magnetic field measurements and to measureme collected using an EEG syste

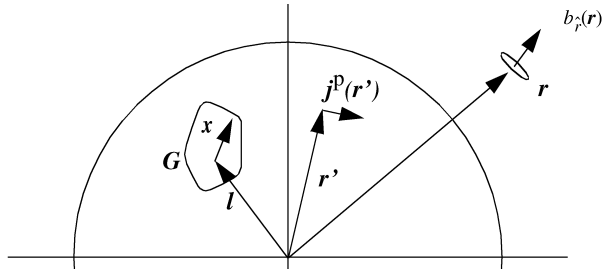

Fig. 1. Primary neural activity of current density $\boldsymbol{j}^p(\boldsymbol{r}')$ at location $\boldsymbol{r}'$ inside a closed conducting volume generates an external magnetic field at location $\boldsymbol{r}$ as detected by a magnetometer with radial orientation $\boldsymbol{r}/r$, to yield the scalar magnetic measurement $b_{\boldsymbol{r}}(\boldsymbol{r})$. We develop a multipolar expansion for sources in a small region, G, using a Taylor series for local displacement $\boldsymbol{x}$

A truncated multipolar expansion will be used to represent the measured magnetic field for the case of a current source restricted to a relatively small volume, G as illustrated in Fig. 1. As the extent of the source grows, more terms are required in the expansion to adequately represent the external magnetic field. In the following we will develop expressions for the special cases of (i) point sources that are exactly represented as *point current dipoles*, (ii) highly focal sources that can be represented by a *magnetic dipole model*, and (iii) locally distributed sources that can be represented by a *first-order multipole model.*

The external magnetic field is generated by the sum of the *primary neural activity*, designated by the current density vector $\boldsymbol{j}^p(\boldsymbol{r'})$, and the *volume* or *return currents* resulting from the electric field produced by the current source. It is the primary currents that are the sources of interest in MEG inverse problems [4]. The contribution of the volume currents to the external field must be accounted for but the currents themselves are of little interest. In the special case treated here of radial measurements for sources confined to a spherical volume, the volume currents do not contribute to the measured field, and the radial component $b_{\boldsymbol{r}}(\boldsymbol{r})$ of the magnetic field $\boldsymbol{b}(\boldsymbol{r})$ at location $\boldsymbol{r}$ is given by direct extension of the well known Biot-Savart equation:

$$b_{\boldsymbol{r}}(\boldsymbol{r}) \equiv \frac{\boldsymbol{r}}{r} \cdot \boldsymbol{b}(\boldsymbol{r}) = \frac{\boldsymbol{r}}{r} \cdot \frac{\mu_0}{4\pi} \int_G \frac{\boldsymbol{r'} \times \boldsymbol{j}^p(\boldsymbol{r'})}{d(\boldsymbol{r}, \boldsymbol{r'})^3} d\boldsymbol{r'} = \frac{\boldsymbol{r}}{r} \cdot \frac{\mu_0}{4\pi} \int_G \frac{\boldsymbol{M}(\boldsymbol{r'})}{d(\boldsymbol{r}, \boldsymbol{r'})^3} d\boldsymbol{r'}, \quad (1)$$

where $\boldsymbol{d}(\boldsymbol{r}, \boldsymbol{r'}) = \boldsymbol{r} - \boldsymbol{r'}$ is the distance vector between the two arguments, $d(\boldsymbol{r}, \boldsymbol{r'}) = \|\boldsymbol{r} - \boldsymbol{r'}\|$ the corresponding scalar distance, and G is any volume containing the source. For the final equality, we define the *magnetic moment density* or *magnetization* as $\boldsymbol{M}(\boldsymbol{r'}) = \boldsymbol{r'} \times \boldsymbol{j}^p(\boldsymbol{r'})$ (e.g., [5](eq. 5.53)).

The multipolar representation is found using the Taylor series expansion of a scalar function

$$\psi(\boldsymbol{r} + \boldsymbol{x}) = \sum_{n=0}^{\infty} (\boldsymbol{x} \cdot \nabla)^n \psi(\boldsymbol{r})/n!, \quad (2)$$

applied to the distance $d(\boldsymbol{r}, \boldsymbol{r'})$, where ∇ represents the gradient with respect to $\boldsymbol{r}$. Using the equalities $\nabla \boldsymbol{r} = \boldsymbol{I}$ (where $\boldsymbol{I}$ is the identity matrix), $\nabla r^n = \nabla(\boldsymbol{r} \cdot \boldsymbol{r})^{n/2} = n r^{n-2} \boldsymbol{r}$, and $\nabla d(\boldsymbol{r}, \boldsymbol{r'})^n = -\nabla' d(\boldsymbol{r}, \boldsymbol{r'})^n = n d(\boldsymbol{r}, \boldsymbol{r'})^{n-2} \boldsymbol{d}(\boldsymbol{r}, \boldsymbol{r'})$ (where ∇' is w.r.t. the primed variable), yields the expansion about $\boldsymbol{r'}$:

$$d(\boldsymbol{r}, \boldsymbol{r'} + \boldsymbol{x})^{-3} = d(\boldsymbol{r}, \boldsymbol{r'})^{-3} + 3d(\boldsymbol{r}, \boldsymbol{r'})^{-5} (\boldsymbol{x} \cdot \boldsymbol{d}(\boldsymbol{r}, \boldsymbol{r'})) + \ldots. \quad (3)$$

To produce the multipolar expansion, we use (3) to expand (1) about $\boldsymbol{r_l}$, the centroid of the region to which the primary source is confined (cf. [6] (eq. 9.3.18)):

$$b_{\boldsymbol{r}}(\boldsymbol{r}) = \frac{\mu_0}{4\pi} \frac{\boldsymbol{r}}{r \|\boldsymbol{r} - \boldsymbol{r_l}\|^3} \cdot \int_G \left(\boldsymbol{M}(\boldsymbol{r_l} + \boldsymbol{x}) + \frac{3\boldsymbol{M}(\boldsymbol{r_l} + \boldsymbol{x})}{\|\boldsymbol{r} - \boldsymbol{r_l}\|^2} \boldsymbol{x} \cdot (\boldsymbol{r} - \boldsymbol{r_l}) + \ldots \right) d\boldsymbol{x}. \quad (4)$$

If $\|\boldsymbol{x}\| \ll \|\boldsymbol{r} - \boldsymbol{r_l}\|$, then we may generally neglect the higher order terms. From Fig. 1 we can see that this inequality is equivalent to the extent of the distributed source being much smaller than the distance from the source to the sensor. We now consider the three types of sources that will be used to represent regions of increasing size in our model of cortical activation.

Point Current Dipole: We consider first the case where the current source is confined to a single point, i.e. $\boldsymbol{j}^p(\boldsymbol{r'}) = \delta(\boldsymbol{r'} - \boldsymbol{r_l})\boldsymbol{q}$ where $\boldsymbol{q}$ is the current dipole moment and δ is the Dirac delta functional. Substitution into (4) produces the result

$$b_{\boldsymbol{r}}(\boldsymbol{r}) = \frac{\mu_0}{4\pi} \frac{\boldsymbol{r} \times \boldsymbol{r_l}}{rd(\boldsymbol{r}, \boldsymbol{r_l})^3} \cdot \boldsymbol{q}, \tag{5}$$

since all terms but the first are identically zero. This is the standard current dipole model that is widely used in the MEG and EEG literature. The source is characterized by the location $\boldsymbol{r_l}$ and moment $\boldsymbol{q}$.

Magnetic Dipole: We now consider the effect of allowing the extent of the source to grow so that it can no longer be represented using a delta function. We let the extent of the source be sufficiently small that the second and higher order terms are negligible, and we rewrite the first term of (4) as

$$b_{\boldsymbol{r}}(\boldsymbol{r}) \cong \frac{\mu_0}{4\pi} \left(\frac{\boldsymbol{r}}{rd(\boldsymbol{r}, \boldsymbol{r_l})^3} \cdot \int_G \boldsymbol{M}(\boldsymbol{r_l} + \boldsymbol{x}) d\boldsymbol{x} \right) = \frac{\mu_0}{4\pi} \frac{\boldsymbol{r}}{rd(\boldsymbol{r}, \boldsymbol{r_l})^3} \cdot \boldsymbol{m}, \tag{6}$$

where we define $\boldsymbol{m}$ to be the *magnetic dipole* moment

$$\boldsymbol{m} = \int_G (\boldsymbol{r_l} + \boldsymbol{x}) \times \boldsymbol{j}^p(\boldsymbol{r_l} + \boldsymbol{x}) d\boldsymbol{x}. \tag{7}$$

Thus we can characterize the magnetic dipole with the moment vector $\boldsymbol{m}$ and location $\boldsymbol{r_l}$. In (7) we can define $\boldsymbol{q}(\boldsymbol{r_l}) = \int_G \boldsymbol{j}^p(\boldsymbol{r_l} + \boldsymbol{x}) d\boldsymbol{x}$ to be the equivalent current dipole moment and $\tilde{\boldsymbol{m}}(\boldsymbol{r_l}) = \int_G \boldsymbol{x} \times \boldsymbol{j}^p(\boldsymbol{r_l} + \boldsymbol{x}) d\boldsymbol{x}$ to be the local magnetic dipole moment, i.e. a local "spin" of the source about a central point. We can therefore express the magnetic moment as $\boldsymbol{m}(\boldsymbol{r_l}) = \boldsymbol{r_l} \times \boldsymbol{q}(\boldsymbol{r_l}) + \tilde{\boldsymbol{m}}(\boldsymbol{r_l})$, and the magnetic dipole includes the equivalent current dipole as the special case.

First-Order Multipole: Now we consider the final case where the source is sufficiently large that the first two terms in the Taylor series should be included. In this case we can rewrite (4) as

$$b_{\boldsymbol{r}}(\boldsymbol{r}) \cong \frac{\mu_0}{4\pi} \frac{\boldsymbol{r}}{rd(\boldsymbol{r}, \boldsymbol{r_l})^3} \cdot \left(\boldsymbol{m} + \frac{3(\boldsymbol{Q}(\boldsymbol{r_l}) \cdot \boldsymbol{d}(\boldsymbol{r}, \boldsymbol{r_l}))}{d(\boldsymbol{r}, \boldsymbol{r_l})^2} \right), \tag{8}$$

where $\boldsymbol{Q}(\boldsymbol{r_l})$ is the *magnetic quadrupolar* term defined as the matrix formed from the tensor product

$$\boldsymbol{Q}(\boldsymbol{r_l}) \equiv \int_G \boldsymbol{M}(\boldsymbol{r_l} + \boldsymbol{x}) \boldsymbol{x} d\boldsymbol{x}. \tag{9}$$

We can rewrite (8) using the Kronecker product $\boldsymbol{a} \otimes \boldsymbol{b}$, defined as the concatenation of the product of each element of $\boldsymbol{a}$ with the vector $\boldsymbol{b}$, and the operator vec($\boldsymbol{A}$), defined as the concatenation of the columns of a matrix into a vector:

$$b_{\boldsymbol{r}}(\boldsymbol{r}) \cong \frac{\mu_0}{4\pi} \left(\frac{\boldsymbol{r}}{rd(\boldsymbol{r}, \boldsymbol{r_l})^3} \cdot \boldsymbol{m} + \frac{3(\boldsymbol{d}(\boldsymbol{r}, \boldsymbol{r_l}) \otimes \boldsymbol{r})}{rd(\boldsymbol{r}, \boldsymbol{r_l})^5} \cdot vec(\boldsymbol{Q}(\boldsymbol{r_l})) \right). \tag{10}$$

We therefore characterize the first-order multipole using the combination of the magnetic dipole moment vector $\boldsymbol{m}$, the nine magnetic quadrupolar terms in $\boldsymbol{Q}(\boldsymbol{r_l})$, and the location $\boldsymbol{r_l}$.

We could obviously continue to expand the multipolar series to higher-order terms. In theory, focal sources could exist such that the leading terms of the expansion integrate to zero, leaving only the higher-order terms. In practice, however, our assumption that the primary activity is modeled as elemental dipoles restricted to the cortex minimizes our need to consider these higher terms. The spatial distance from the cortex to the sensors, the relative smoothness of the cortical surface, and the relatively high noise levels suppress these higher-order moments in relatively focal regions of activation.

2.2 The Forward Problem

The multipolar development above includes three models of assumed increasing spatial extent, each of which produces a radial magnetic field measurement which is a nonlinear function of the location (i.e. the center of expansion for the Taylor series) and a linear function of its moments. In the inverse problem, both the linear and nonlinear terms are assumed unknown. The decomposition into linear and nonlinear components for the current dipole model has previously been used to simplify nonlinear least squares fitting [9] and localization using signal subspace methods such as MUSIC [7,8]. Since the magnetic dipole and first order multipole are similarly decomposed, these methods can be directly extended to include searches for distributed non-dipolar sources. Furthermore, as noted above, the expansions included here can be readily extended to the case of non-radial MEG and EEG measurements for the spherical head models.

The radial magnetic field can be represented for each of the three types of source as the inner product of a *gain* vector and the vector of linear parameters, $b(\boldsymbol{r}) = \boldsymbol{g}(\boldsymbol{r}, \boldsymbol{r_l}) \cdot \boldsymbol{l}$. The separation of nonlinear and linear parameters are clearly shown in (5), (6), and (10). We assume an MEG array of m sensors sampling the magnetic field of the source. By concatenating these measurements into a vector, we can represent the "forward field" of the source as

$$\left[b(\boldsymbol{r}_1) \ldots \ b(\boldsymbol{r}_m) \right]^T = \left[\boldsymbol{g}(\boldsymbol{r}_1, \boldsymbol{r_l}), \ldots, \boldsymbol{g}(\boldsymbol{r}_m, \boldsymbol{r_l}) \right]^T \boldsymbol{l} = \boldsymbol{G}(\boldsymbol{r_l})\boldsymbol{l} \tag{11}$$

where $\boldsymbol{G}(\boldsymbol{r_l})$ is the "gain matrix" which accounts for all possible orientations of the source at $\boldsymbol{r_l}$ [9]. The forward model for an arbitrary combination of sources can be found by linear superposition. To extend the forward model to include temporal variations, we adopt the assumption that there are a finite combination

of sources that are active. The solution of the inverse involves estimating the location, moment parameters and time courses of each of these sources.

It is possible for two sources to be synchronous. For example, bilateral activation in sensory or auditory cortex could be represented by two synchronous focal dipoles, one in each hemisphere. To account for this possibility in the subspace methods described below, we adopt an *independent topography model* [7] in which each topography consists of one or more elementary sources, all of which have identical time courses. For a *p-source topography* sampled over m sensors and n time instances, we may express the resulting $m \times n$ spatiotemporal data matrix as

$$\begin{bmatrix} b(\boldsymbol{r}_1, t_1) & \cdots & b(\boldsymbol{r}_1, t_n) \\ \vdots & \ddots & \vdots \\ b(\boldsymbol{r}_m, t_1) & \cdots & b(\boldsymbol{r}_m, t_n) \end{bmatrix} = \left[\boldsymbol{G}(\boldsymbol{r}_{\boldsymbol{l}_1}), \cdots, \boldsymbol{G}(\boldsymbol{r}_{\boldsymbol{l}_p}) \right] \begin{bmatrix} \boldsymbol{l}_1(t_1) & \cdots & \boldsymbol{l}_1(t_n) \\ \vdots & \ddots & \vdots \\ \boldsymbol{l}_p(t_1) & \cdots & \boldsymbol{l}_p(t_n) \end{bmatrix} \quad (12)$$

where $\boldsymbol{l}_j(t_k)$ represents the linear parameters for the jth source sampled at the kth time instance. Since all of these sources have the same time course, the matrix of linear parameters is rank one and may be decomposed using an SVD into the outer product of a single pair of singular vectors $\boldsymbol{u}$ and $\boldsymbol{v}$ scaled by the singular value σ,

$$\boldsymbol{u}\sigma\boldsymbol{v}^T = \begin{bmatrix} \boldsymbol{l}_1(t_1) & \cdots & \boldsymbol{l}_1(t_n) \\ \vdots & \ddots & \vdots \\ \boldsymbol{l}_p(t_1) & \cdots & \boldsymbol{l}_p(t_n) \end{bmatrix}. \quad (13)$$

Defining the scalar time series of this independent topography to be $\boldsymbol{s} = \sigma\boldsymbol{v}$, we may rewrite (12) as

$$\left[\boldsymbol{G}(\boldsymbol{r}_{\boldsymbol{l}_1}) \cdots \boldsymbol{G}(\boldsymbol{r}_{\boldsymbol{l}_p}) \right] \boldsymbol{u} \left[s(t_1), \cdots, s(t_n) \right] = \boldsymbol{a}(\rho_1, \boldsymbol{u}_1)\boldsymbol{s}^T. \quad (14)$$

The p-source topography vector is a function of the set ρ_1 of p source locations, $\rho_1 = \{\boldsymbol{r}_{\boldsymbol{l}_i}\}$, $i = 1, \ldots, p$ and the unit norm vector $\boldsymbol{u}_1$ from (13). The vector $\boldsymbol{u}_1$ may be viewed as a generalization of an "orientation" vector by concatenating all of the linear source parameters and scaling by its length,

$$\boldsymbol{u}_l \equiv \left[\boldsymbol{l}_1^T, \ldots, \boldsymbol{l}_p^T \right]^T / \left\| \left[\boldsymbol{l}_1^T, \ldots, \boldsymbol{l}_p^T \right] \right\|. \quad (15)$$

To complete the full model for the observed MEG data we simply concatenate the r independent topographies that make up the complete source and add noise:

$$\boldsymbol{F} = \boldsymbol{A}(\rho, \boldsymbol{u})\boldsymbol{S}^T + \boldsymbol{N} = \left[\boldsymbol{a}(\rho_1, \boldsymbol{u}_1), \ldots, \boldsymbol{a}(\rho_r, \boldsymbol{u}_r) \right] \begin{bmatrix} \boldsymbol{s}_1^T \\ \vdots \\ \boldsymbol{s}_r^T \end{bmatrix} + \boldsymbol{N}, \quad (16)$$

where each $m \times 1$ column vector $\boldsymbol{a}(\rho_i, \boldsymbol{u}_i) \equiv \boldsymbol{G}(\rho_i)\boldsymbol{u}_i$ represents the ith independent topography corresponding to the ith time series $\boldsymbol{s}_i$. The set ρ comprises

the r sets of source locations $\{\rho_i\}$ and the set $\boldsymbol{u}$ the corresponding topography orientations $\{\boldsymbol{u}_i\}$. Each topography may comprise one or more multipolar sources, but only a single time series. By our definition of independent topographies, the matrix of time series $\boldsymbol{S}$ is rank r, and the matrix of topographies $\boldsymbol{A}$ is assumed to be unambiguous and also of rank r. The matrix $\boldsymbol{N}$ represents additive random noise, which we will assume to be spatially and temporally white with zero mean and variance σ_e^2.

2.3 Signal Subspace

Under the assumption that the signal is uncorrelated with the noise, the autocorrelation matrix for the $m \times n$ spatiotemporal data in (16) is

$$\boldsymbol{R} = E\{\boldsymbol{F}\boldsymbol{F}^T\} = \boldsymbol{A}(\boldsymbol{S}^T\boldsymbol{S})\boldsymbol{A}^T + n\sigma_e^2\boldsymbol{I}. \tag{17}$$

The autocorrelation matrix can expressed using an eigendecomposition as:

$$\boldsymbol{R} = [\boldsymbol{\Phi}_s|\boldsymbol{\Phi}_e] \begin{bmatrix} \boldsymbol{\Lambda}_s & \boldsymbol{0} \\ \boldsymbol{0} & \boldsymbol{\Lambda}_e \end{bmatrix} [\boldsymbol{\Phi}_s|\boldsymbol{\Phi}_e]^T \tag{18}$$

where the diagonal matrix $\boldsymbol{\Lambda}_s = \boldsymbol{\Lambda} + n\sigma_e^2\boldsymbol{I}$ represents the r largest "signal plus noise" eigenvalues and their corresponding eigenvectors form the matrix $\boldsymbol{\Phi}_s$. The diagonal matrix $\boldsymbol{\Lambda}_e = n\sigma_e^2\boldsymbol{I}$ represents the smallest "noise" eigenvalues and their corresponding eigenvectors form the matrix $\boldsymbol{\Phi}_e$.

We refer to $\boldsymbol{\Phi}_s$ as spanning the *signal subspace* and to $\boldsymbol{\Phi}_e$ as spanning the *noise-only subspace*. In practice, we estimate the signal $\boldsymbol{\Phi}_s$ and noise $\boldsymbol{\Phi}_e$ subspace basis vectors by a eigendecomposition of the outer product $\boldsymbol{F}\boldsymbol{F}^T$ or an SVD of $\boldsymbol{F}$. We denote the estimate of $\boldsymbol{\Phi}_s$ as $\hat{\boldsymbol{\Phi}}_s$.

3 Source Localization

3.1 RAP-MUSIC

The RAP-MUSIC algorithm is described in detail in [8]. Here we briefly review the method and describe its application in combination with the multipolar models developed above. The first source is found at the location which produces the global maximum of the metric

$$\rho_1 = \arg\max(subcorr(\boldsymbol{G}(\rho), \hat{\boldsymbol{\Phi}}_s)_1). \tag{19}$$

The function $subcorr(\cdot)$ represents the "subspace correlations" between the two matrices. The subspace correlations are the ordered set of cosines of the principal angles as defined in [3]. The first subspace correlation, $subcorr(\cdot)_1$, corresponds to the cosine of the smallest principal angle and will be unity if the two matrices have at least a one-dimensional subspace in common. If we define $\boldsymbol{U}_{\boldsymbol{G}}$ to be

the orthogonal matrix spanning the same space as $\boldsymbol{G}(\rho)$, then the square of the subspace correlations are found as the eigenvalues of the matrix

$$\boldsymbol{U}_{\boldsymbol{G}}^{T}\hat{\boldsymbol{\Phi}}_{s}\hat{\boldsymbol{\Phi}}_{s}^{T}\boldsymbol{U}_{\boldsymbol{G}}. \tag{20}$$

By maximizing the first subspace correlation in (19), we identify the source location and corresponding gain matrix that has the smallest principal angle with respect to the signal subspace. Since we only need to search over the location parameter, a nearly exhaustive search over a relatively dense three-dimensional grid within the brain volume can be performed relatively quickly for any of the three source models of the previous section. For the case of synchronous sources, the dimensionality of the search increases by at least a factor of two and the computational cost rises dramatically, but the procedure nonetheless proceeds directly.

To complete the first independent topography model, we need the corresponding source orientation vector, which is a simple linear transformation of the eigenvector of (20) corresponding to the maximum eigenvalue [3,7]. The resulting estimates yield the first estimated independent topography, $\boldsymbol{a}(\hat{\rho}_1, \hat{\boldsymbol{u}}_1) = \boldsymbol{G}(\hat{\rho}_1)\hat{\boldsymbol{u}}_1$.

For each of the remaining $k = 1, 2, \ldots, r$ RAP-MUSIC recursions, the nonlinear source location parameters are found as

$$\hat{\rho}_k = \arg\max \left(subcorr \left(\boldsymbol{\Pi}^{\perp}_{\hat{\boldsymbol{A}}_{k-1}} \boldsymbol{G}(\rho), \boldsymbol{\Pi}^{\perp}_{\hat{\boldsymbol{A}}_{k-1}} \hat{\boldsymbol{\Phi}}_{s} \right)_1 \right) \tag{21}$$

where $\hat{\boldsymbol{A}}_{k-1} = [\boldsymbol{a}(\hat{\rho}_1, \hat{\boldsymbol{u}}_1), \ldots, \boldsymbol{a}(\hat{\rho}_{k-1}, \hat{\boldsymbol{u}}_{k-1})]$ represents the composite independent topography matrix, and the projection operator $\boldsymbol{\Pi}^{\perp}_{\hat{\boldsymbol{A}}_{k-1}}$ is computed as

$$\boldsymbol{\Pi}^{\perp}_{\hat{\boldsymbol{A}}_{k-1}} = \boldsymbol{I} - \hat{\boldsymbol{A}}_{k-1}\hat{\boldsymbol{A}}^{\dagger}_{k-1} \tag{22}$$

where $\hat{\boldsymbol{A}}^{\dagger}_{k-1} \equiv (\hat{\boldsymbol{A}}^{T}_{k-1}\hat{\boldsymbol{A}}_{k-1})^{-1}\hat{\boldsymbol{A}}^{T}_{k-1}$ is the pseudoinverse of $\hat{\boldsymbol{A}}_{k-1}$. Through this recursion, we sequentially remove the components of the signal subspace that can be explained by the sources that have already been found. We then search the remaining signal subspace for additional sources.

At each iteration the source location set ρ in (21) may represent one or more multipolar sources. To find the simplest sources consistent with the data, we begin the search with the current dipole model, then progress through the magnetic and first-order multipole models. The decision to increase the complexity of the model is based on a minimum correlation threshold. In this paper, we will restrict the search to one-source models only, halting the recursion when the first-order multipole maximum subspace correlation drops too low. Examples of different correlation thresholds are given in the Monte Carlo simulations in the next section. Extensions to multiple synchronous dipolar sources are discussed in [7], with obvious extensions to multiple multipolar sources.

With all sources in the data identified and their independent topographies represented in the final topography matrix $\hat{\boldsymbol{A}}_r$, estimates of the corresponding time series are readily found as $\hat{\boldsymbol{S}} = (\hat{\boldsymbol{A}}_r{}^{T}\hat{\boldsymbol{A}}_r)^{-1}\hat{\boldsymbol{A}}_r{}^{T}\boldsymbol{F}$ or in some regularized form thereof.

3.2 Mapping Parametric Sources onto Cerebral Cortex

The linear parameters of the multipolar model computed using the RAP-MUSIC search are estimates of the moments formed by integrating the primary current sources as defined in (1). When the sources are confined to cortex, which we can represent as a continuous surface, the moments are generated as integrals over a surface patch containing the sources. For the single-source topographies considered here, we assume that each source represents the activation of a single contiguous cortical patch. The final step in our parametric imaging method is then to relate the multipolar moments back to a plausible distribution on the cortical surface which consists of a set of patches of activation consistent with the estimated moments. Fitting the moments to sources on the cortex involves estimation of both the surface patch and the current distribution on that patch. As with the original MEG inverse problem, the solutions are ambiguous. However, under the assumption that each surface patch is contiguous and in the vicinity of the estimated multipole, the degree of ambiguity is greatly reduced.

To perform the final stage of the multipolar imaging method we use a finely tesselated cortical surface extracted from an MRI volume. In fitting the multipolar sources to the cortex, we allow a current element at the vertex of each triangular patch on the surface, with an orientation derived as a weighted sum of the triangular normals adjacent to the vertex. To fit a specific multipolar source with topography $\boldsymbol{a}(\rho_i, \boldsymbol{u}_i)$ to the cortical surface, we begin by creating a list of candidate locations on the cortex in the vicinity of the source location. For each candidate point, we test the subspace correlation between the point and the topography. If the point with the highest correlation meets a minimum threshold (e.g. 98%), we designate it as the corresponding re-mapped cortical source for that topography and halt. Otherwise, we add adjacent points to each of the candidate points to form small distributed patches and continue to swell each candidate point until we find a patch that meets the threshold.

This approach will generate a patch of minimal size consistent with the identified topography. We may continue to swell the patch and find additional possible sources consistent with the topography, a consequence of the ambiguity in the inverse problem rather than a specific limitation of the method described. Currently we grow the patch by adding a ring of triangles around the elements already in the patch. A more sophisticated approach based on testing a number of possible candidates to add to each patch may prove more robust. Alternatively, we could adopt a stochastic model for the mapping between the estimated multipolar parameters and the corresponding cortical activation. This approach could readily incorporate the activation models described in our previous work on Bayesian MEG imaging [11].

4 Monte Carlo Simulations

In the first simulation we used the tesselated human cortex shown in Fig. 2 which contains approximately 230,000 triangles. Radial magnetic fields sensors and a spherical forward model were used in the generation of the simulated

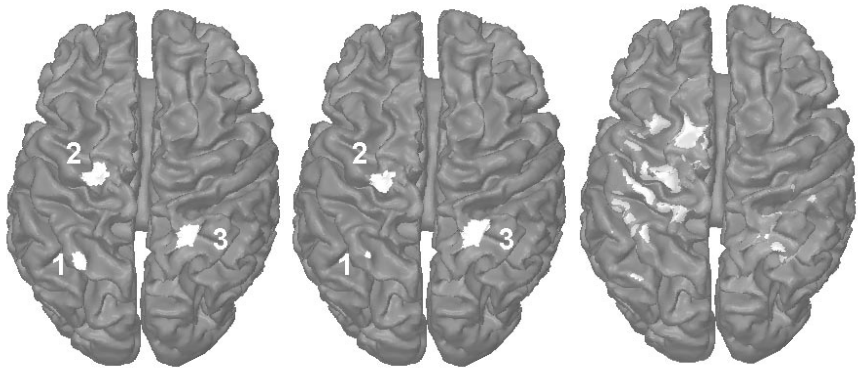

Fig. 2. (a) The ground truth for the simulation study showing mappings of the three sources onto the cortical surface; (b) Reconstruction of the cortical activity using the multipolar method; (c) Reconstruction of the data from time $t = 10$ using a regularized minimum L_2 norm method

data and in the inverse method. Three distributed sources were created on the cortical surface, also shown in Fig. 2. The three sources were given overlapping independent time courses as shown in Fig. 3. The forward magnetic field was measured by a simulated array of 104 magnetometers spaced approximately uniformly on the upper hemisphere at a radius of 12 cm. Zero mean Gaussian white noise was added to the sensor data at a ratio of 100:1 signal to noise variance.

Although analysis of the singular value spectrum of this high SNR data clearly revealed a rank of three, we overspecified the rank to ten to demonstrate robustness to selecting too great a rank. We set the acceptance threshold for correlation at 98%. The RAP-MUSIC algorithm was first run with the simplest of the source topographies, the current dipole (5), for which a maximum correlation of 99.9% was found. On the second recursion, the correlation with the dipole model dropped below the threshold of 98%. We therefore increased the complexity of the model to the magnetic dipole (6) and achieved a correlation of 98.3%. The third recursion was below the threshold for the magnetic dipole, so we increased the model to a first-order multipole (10) to obtain a correlation of 99.9%. On the fourth recursion, the correlation plummeted to 62% for the multipole and the recursion was halted at three sources. The three topographies found were then used in a least-squares fit to determine the time series of the three sources, Fig. 3.

We mapped the three topographies into the minimal cortical source regions, also shown in Fig. 2. For comparison we also include a regularized minimum L_2-norm solution fitted at one of the intermediate time slices, for which the spatial distribution and time series are also shown in Fig. 2 and Fig. 3. We see that although the re-mapped topographies obtained using the multipolar method are not identical to the "ground truth" they are indeed similar. In comparison,

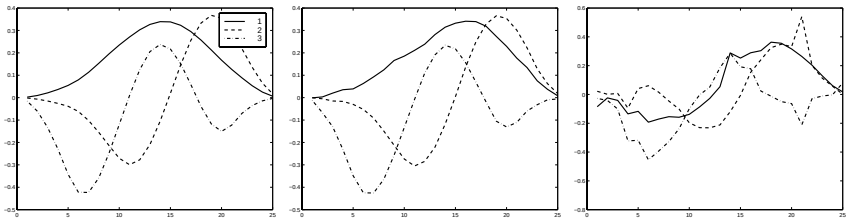

Fig. 3. Time courses for the three sources (a) ground truth; (b) time courses estimated using the multipolar method; (c) time courses averaged over each of the true activation areas computed from the minimum norm solutions. In this high SNR example, the time series reconstruction in (b) is nearly perfect, while (c) exhibits high noise sensitivity

the minimum norm solution exhibits substantial source blurring due to the low resolution of the linear inverse methods.

As discussed above, the multipolar source center is assumed to be near the distributed cortical source. We tested this assumption in a Monte Carlo simulation of 10,800 distributed sources over a range of noise levels. We also tested the effects of the correlation threshold parameter used in the RAP-MUSIC algorithm to accept a model. Each source was centered randomly on the upper half of the brain surface in Fig. 2. With a 50% probability, each source was either a "monophasic" contiguous patch of 200 mm^2 or a "biphasic" patch of two 200 mm^2 patches centered about 8 mm apart (about 50% overlap) and of opposite polarity. Each Monte Carlo realization simulated three such sources with overlapping non-orthogonal time series. No attempt was made to force the three sources to be widely separated, so that source overlaps were possible in any single realization. A hemispherical array of 138 magnetometers was simulated a few centimeters above the cortical surface. Although the true signal subspace rank was three, we intentionally selected a larger rank of five for each realization.

Twelve cases of SNR and correlation threshold were tested, with 300 Monte Carlo realizations per case, for a total number of 10,800 sources. For each simulated source, we determined the geometric centroid of the patch. We then computed the distance from this centroid to the multipolar source location nearest to the source as an indication of the accuracy of the estimate. However, we note that the multipole that gives the best fit to a particular distributed cortical source does not necessarily lie *on* the cortex.

The global statistics presented in Table 1 show that the current dipolar locations are in general closer to the patch centroids than the non-dipolar locations. The 20 dB SNR case represents a mostly noiseless signal to allow observations of the modeling effects. Even though the sources were spatially large, the majority of the monophasic and some of the biphasic sources were modeled quite well as dipoles, even at the 99% correlation level. The first-order multipole model accounted for the remainder. The 3 dB SNR case represents a rather severe case of 67% signal variance to 33% noise variance. At 99% correlation, most sources

Table 1. Monte Carlo Study. SNR is ten times the log base-ten of the ratio of the total signal variance to the total noise variance, both values measured at the array of sensors. Correlation threshold is the minimum subspace correlation value for the model to be accepted. The first row summarizes the results over all trials for a total of 10,800 sources localized. Each additional row represents a different Monte Carlo trial of 300 realizations and 900 sources. The sources are described in the text. The mean and standard deviation (in mm) for the solution distances are given for the ECD model and the non-ECD (magnetic dipoles and first-order multipoles combined). The final column gives the number not localized at the given threshold.

SNR (dB)	Correlation Threshold	Number of ECDs	Mean, Std.Dev	Non-ECDs	Mean, Std.Dev	Missing Sources
ALL	ALL	6659	(5.34, 4.56)	2977	(7.06, 5.98)	1164
3	0.94	643	(6.51, 5.38)	183	(6.05, 5.81)	74
3	0.96	565	(5.69, 4.03)	215	(6.28, 6.58)	120
3	0.98	378	(5.17, 3.88)	282	(7.25, 6.59)	240
3	0.99	65	(6.32, 3.98)	220	(14.58, 8.37)	615
10	0.94	698	(6.35, 5.81)	198	(4.85, 6.70)	4
10	0.96	641	(5.68, 4.86)	254	(4.43, 5.55)	5
10	0.98	575	(4.47, 3.15)	302	(4.20, 3.41)	23
10	0.99	489	(3.99, 2.86)	332	(4.41, 3.57)	79
20	0.94	737	(6.03, 5.60)	163	(4.99, 6.72)	0
20	0.96	702	(4.97, 4.17)	198	(4.73, 5.27)	0
20	0.98	625	(4.69, 3.94)	275	(3.96, 3.56)	0
20	0.99	541	(4.26, 3.38)	355	(3.96, 2.97)	4

are lost in the noise, but at the lower correlation thresholds we see the majority of sources still detected quite well as either dipoles or multipoles. Although we intentionally set too large a rank for the signal subspace, we also note the important fact that no spurious sources were found, i.e. we never saw more than three sources. As we might expect, the effect of lowering the correlation threshold is to allow more sources to be detected, but at the cost of greater mean distance between the source locations and the patch centroids.

5 Conclusion

We have described an algorithm for computing estimates of cortical current activity from MEG data. The method exploits the low dimensionality of parametric multipolar models to estimate the locations of equivalent representations of the current sources. These representations are then mapped onto a tessellated representation of the cortical surface resulting in a spatiotemporal estimate of cortical activity. Monte Carlo simulations indicate that the potential of this method to extend the parametric approach to the representation of more distributed sources. The resulting images avoid the very low resolution encountered using minimum norm methods and the high computational costs of the other

nonlinear imaging methods. Planned studies include experimental phantoms and human studies of self paced and visually cued motor activation.

Acknowledgements: This work was supported in part by the National Institute of Mental Health Grant RO1-MH53213 and the Los Alamos National Laboratory, operated by the University of California for the United States Department of Energy under contract W-7405-ENG-36. S.B. is a laureate of the Lavoisier research fellowship from the French Ministry of Foreign Affairs.

References

1. Baillet, S., Garnero, L.: A Bayesian approach to introducing anatomo-functional priors in the EEG/MEG inverse problem. IEEE Trans. Biomed. Eng., **44** (1997) 374–385
2. Dale, A.M., Sereno, M.I.: Improved localization of cortical activity by combining EEG and MEG with MRI cortical surface reconstruction: a linear approach. J. Cog. NeuroSci., **5** (1993) 162–176
3. Golub G.H., Van Loan, C.F.: Matrix Computations, Second Edition. Johns Hopkins University Press, (1984).
4. Hämäläinen, M., Hari, R., Ilmoniemi, R.J., Knuutila, J., Lounasmaa, O.V.: Magnetoencephalography-theory, instrumentation, and applications of noninvasive studies of the working human brain. Rev. Mod. Phys., **65** (1993) 413–497
5. Jackson, J.D.: Classical Electrodynamics, Second Edition. John Wiley and Sons, New York, (1975).
6. Katila, T., Karp, P.: Magnetocardiography: Morphology and multipole presentations. In: Williamson, S.J., Romani, G.-L., Kaufman, L., Modena, I. (eds.): Biomagnetism, An Interdisciplinary Approach. Plenum, New York (1983) 237–263
7. Mosher, J.C., Leahy., R.M.: Recursive music: A framework for EEG and MEG-source localization. IEEE Trans. Biomed. Eng., **45** (1998) 1342–1354
8. Mosher, J.C., Leahy., R.M.: Source localization using recursively applied and projected (RAP) MUSIC. IEEE Trans. Signal Proc., **47** (1999) 332–340.
9. Mosher, J.C., Lewis, P.S., Leahy, R.M.: Multiple dipole modeling and localization from spatio-temporal MEG data. IEEE Trans. Biomed. Eng., **39** (1992) 541–557
10. de Munck, J.C., van Dijk B.W., Spekreijse H.: Mathematical dipoles are adequate to describe realistic generators of human brain activity. IEEE Trans. on Biomedical Engineering, **35** (1988) 960–966
11. Phillips, J.W., Leahy, R.M., Mosher, J.C.: MEG-based imaging of focal neuronal current sources. IEEE Trans. on Medical Imaging, **16** (1997) 338–348
12. Scherg, M., von Cramon, D.: Two bilateral sources of the late AEP as identified by a spatiotemporal dipole model. Electroenceph. and Clin. Neurophys., **62** (1985) 32–44
13. R.O. Schmidt.: Multiple emitter location and signal parameter estimation. IEEE Trans. on Ant. and Prop., **AP-34** (1986) 276–280
14. Wang, J. Z., Williamson, S. J., Kaufman, L.: Magnetic source images determined by a lead-field analysis: The unique minimum-norm least-squares estimation. IEEE Trans. Biomed. Eng., **39** (1992) 665–675.
15. Wikswo, J.P.: Biomagnetic sources and their models, In: Williamson, S.J., Hoke, M., Stroink G., Kotani M. (eds.): Advances in Biomagnetism. Plenum, New York (1989).